

207 NEW OPEN STAR CLUSTERS WITHIN 1 KPC FROM GAIA DATA RELEASE 2

GYUHEON SIM¹, SANG HYUN LEE^{2,3}, HONG BAE ANN⁴, AND SEUNGHYEON KIM¹

¹Ulsan Science High School, Ulsan, 44902, Korea; 2017000049@ushs.hs.kr, 2017000016@ushs.hs.kr

²Korea Astronomy and Space Science Institute, Daejeon 34055, Korea; shlee@ksai.re.kr

³Department of Physics, University of Ulsan, Ulsan 44610, Korea

⁴Pusan National University, Busan 46241, Korea; hbann@pusan.ac.kr

Received May 14, 2019; accepted July 16, 2019

Abstract: We conducted a survey of open clusters within 1 kpc from the Sun using the astrometric and photometric data of the *Gaia* Data Release 2. We found 655 cluster candidates by visual inspection of the stellar distributions in proper motion space and spatial distributions in $l - b$ space. All of the 655 cluster candidates have a well defined main-sequence except for two candidates if we consider that the main sequence of very young clusters is somewhat broad due to differential extinction. Cross-matching of our 653 open clusters with known open clusters in various catalogs resulted in 207 new open clusters. We present the physical properties of the newly discovered open clusters. The majority of the newly discovered open clusters are of young to intermediate age and have less than ~ 50 member stars.

Key words: open clusters and associations: general — catalogs — methods: data analysis

1. INTRODUCTION

Open clusters are local concentrations of stars with a common sense of motion (Trumpler 1931). They are thought to have been formed in the same nebulae. Trumpler (1930) classified open clusters into four types according to central concentration, luminosity range of member stars, and number of cluster members. Open clusters are good tracers of the Galactic structure (Janes & Adler 1982; Janes & Phelps 1994) as well as test beds for stellar evolution theory (e.g. Sandage 1957; Mermilliod 1981) and dynamics of stellar systems (Terlevich 1987). However, owing to severe contamination of cluster images with field stars, it is challenging to determine their sizes and morphologies. Evaporation of low mass stars as part of the dynamical evolution of star clusters makes it difficult to distinguish member stars in the outer regions of clusters from field stars even if kinematic data are available (Frinchaboy & Majewski 2008).

Multiple catalogs of open clusters are available. The Lund Catalogue of Open Cluster Data (Lynga 1987) lists about 1200 open clusters which have been intensively used as targets of photometric surveys such as that of Ann et al. (1999). Dias et al. (2002) compiled 1537 open clusters, updating previous catalogs including those of Lynga (1987) and Mermilliod (1995). After publications of the DALM catalog by Dias et al. (2002), multiple studies aimed at discovering new open clusters by analyzing stellar catalogs such as the All-Sky Compiled Catalogue (ASCC-2.5) (Kharchenko 2001; Röser, Demleitner & Schilbach 2010). Kharchenko et al. (2005) discovered 109 new open clusters using the ASCC-2.5 while Scholz et al. (2015) discovered 63 new open clusters using the PPXML catalog (Röser, Demleitner & Schilbach 2010). Both catalogs are all sky catalogs that provide positions

and proper motions in the International Celestial Reference System (ICRS) together with the near-infrared magnitudes from 2MASS (Skrutskie et al. 2006) for 399 million objects. These new discoveries were a by-product of constructing the Catalogue of Open Cluster Data (COCD) from ASCC-2.5 and the global Milky Way Star Clusters (MWSC) survey which compiled ~ 3000 clusters from PPXML. The work of Mermilliod (1995) has evolved into the WEBDA database.¹ DALM is continuously updated and lists about 2000 open clusters to date.

Until recently, visual inspections of photographic plates or CCD images were the most widely used method to search for open clusters. However, there are two notable movements in this field: extension to other wavelengths, and computer-aided search. Infrared observations have been quite successful in finding embedded clusters (Camargo, Bica & Bonatto 2015a; Camargo et al. 2015b; Ryu & Lee 2018; Oliveira, Bica & Bonatto 2018). Embedded clusters are groups of very young stars that are partially or fully obscured by interstellar gas and dust. Computer-aided search applies automated search algorithms to large stellar databases. Koposov, Belokurov & Torrealba (2017) detected a new star cluster by analyzing overdensity in spatial distributions of all sources in the *Gaia* Data Release 1 (Gaia Collaboration et al. 2016b). More elaborated algorithms such as UP-MASK (Krone-Martins & Moitinho 2014) were applied to the *Gaia* data with notable success (Castro-Ginard et al. 2018; Cantat-Gaudin et al. 2019).

The *Gaia* mission (Gaia Collaboration et al. 2016a) has made available highly precise astrometric measurements of more than one billion stars along with precise magnitudes in three passbands – G (330 nm–1050 nm), G_{BP} (330 nm–680 nm), and G_{RP} (630 nm–1050 nm).

CORRESPONDING AUTHOR: H. B. Ann

¹<https://webda.physics.muni.cz>

Table 1
Size of search area.

$ b (^{\circ})$	<15	15–21	21–30	30–80	80–90
Area	$2^{\circ} \times 2^{\circ}$	$3^{\circ} \times 3^{\circ}$	$9^{\circ} \times 9^{\circ}$	$10^{\circ} \times 10^{\circ}$	$90^{\circ} \times 10^{\circ}$

The second release of *Gaia* data (*Gaia* DR2) provides celestial coordinates, proper motions and parallaxes of about 1.3 billion stars along with photometric magnitudes (Gaia Collaboration et al. 2018). *Gaia* DR2 data have been used to find new open clusters in multi-dimensional parameter spaces. Castro-Ginard et al. (2018) and Cantat-Gaudin et al. (2019) found 31 and 41 open clusters from *Gaia* DR2 using the cluster-finding algorithms DBSCAN and UPMASK, respectively. Cantat-Gaudin et al. (2019) utilized a Gaussian mixture model (GMM) along with UPMASK to detect star clusters. Application of UPMASK to the astrometric data of *Gaia* DR2 for 3328 open clusters compiled from various catalogs in the literature, including those of Froebrich, Scholz & Raftery (2006), Kharchenko et al. (2013), and Dias et al. (2002), yielded the identification of 1229 open clusters (Cantat-Gaudin et al. 2018).

Due to dynamical evolution, open clusters can change in morphology and size. They also can be disrupted by encounters with giant molecular clouds (Gieles et al. 2006) and flattened by Galactic tidal forces (Terlevich 1987). Elongated morphologies have been reported for some clusters such as the Hyades (Oort 1979) and Pleiades (Raboud & Mermilliod 1998). The Galactic tidal field can stretch clusters towards the Galactic center. In addition, elongation is frequent in young open clusters (e.g. Chen et al. 2004), indicating a link to cluster formation processes. Numerical simulations explicitly showed the role of dynamical evolution for elongation (Kharchenko et al. 2009). Tidal tails have been predicted to be aligned with the Galactic orbit (Chumak et al. 2010). Lee, Kang & Ann (2013) found the weak signature of a tidal tail in the open cluster NGC 1245 from a statistical analysis of deep CCD photometry. Recently, observational evidence of the Hyades tidal tails was reported (Röser, Schilbach & Goldman 2019).

The aim of this study is to find new open clusters within 1 kpc from the Sun by visual inspection using multi-dimensional data of *Gaia* DR2. Recent discoveries of open clusters from *Gaia* DR2 were made through automated algorithms. However, most open clusters have been found visually. We expect that visual inspection of clustering patterns in proper motion space and spatial distribution of stars will discover many open clusters not yet identified. In addition, the precision of the *Gaia* astrometric data greatly reduces the difficulties in distinguishing cluster stars from background field stars. Since we restricted our survey to the stars within 1 kpc, we reach down to the faint main-sequence stars which are required to examine the outer regions of open clusters. We anticipate that the information of the outer structures of open clusters will greatly help us to broaden

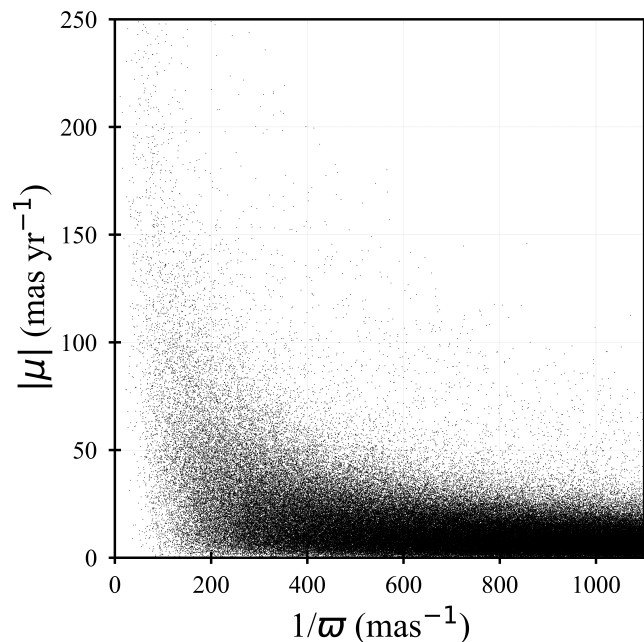


Figure 1. Proper motion vs. parallax of sample stars.

our view of the dynamical evolution of open clusters, field star formation, and structure of the Milky Way.

This paper is organized as follows. In Section 2, we explain the *Gaia* DR2 data and the selection criteria used to extract the *Gaia* DR2 data while minimizing field star contamination. In Section 3, we describe how we found clusters visually, validated clusters with the PARSEC set of metallicity $Z = 0.02$ isochrones (Bressan et al. 2012) and derived their parameters quantitatively. In Section 4, we present our catalog of newly found clusters with a brief description of the properties of the new clusters. Finally, in Section 5, we summarize and discuss our results.

2. DATA

The *Gaia* DR2 is based on data collected during the first 22 months of the nominal mission lifetime. The biggest difference between DR1 and DR2 is that DR2 provides photometric data suitable for constructing color-magnitude diagrams (CMD) of clusters. We used the five astrometric parameters Galactic longitude l , Galactic latitude b , proper motion in right ascension $\mu_{\alpha} \cos \delta$ (with δ being the declination), proper motion in declination μ_{δ} , parallax angle ϖ , and the three *Gaia* photometric magnitudes, G , G_{BP} , and G_{RP} to search for open clusters. In general, the typical uncertainty of the astrometric measurements increases as the target brightness decreases. The typical uncertainties in position and parallax are ~ 0.04 mas for bright sources ($G < 14$ mag) and 0.7 mas at $G = 20$ mag (Lindegren et al. 2018). Along with these typical uncertainties, there is a zero-point offset (-0.029 mas) in the *Gaia* parallaxes (Lindegren et al. 2018). We corrected our cluster distances for the zero-point offset. Another source of uncertainty is an offset in the G_{BP} and G_{RP} magnitudes at the faint end ($G > 19$) of the *Gaia* data (Gaia

Collaboration et al. 2018).

As described in Gaia Collaboration et al. (2018), there are some sources that have spurious parallaxes. Most of them are faint sources and concentrated in dense regions along the Galactic plane and towards the bulge of the Galaxy (Lindegren et al. 2018). Since the uncertainty in a parallax propagates into the estimates for distance-related parameters, it is better to exclude faint stars from the sample and to keep in mind the possibility of spurious parallaxes for stars in dense regions. By considering the uncertainties in the five astrometric parameters of *Gaia* DR2, we selected stars brighter than $G = 18$ mag with parallaxes $\varpi > 0.833$ mas. For our magnitude cut, the errors in position and parallax are about 0.15 mas, errors in proper motion are about 0.3 mas yr^{-1} . Errors of this magnitude have little impact on the identification of clusters in the multi-dimensional parameter space described below as they correspond to less than $\sim 10\%$ of the mean proper motions and parallaxes of candidate clusters, respectively. A brightness cut $G < 18$ is necessary because large errors in positions and parallaxes of faint stars make the visual detection of sparse clusters difficult. Figure 1 presents the relationship between proper motion and parallax, showing that most of the sample stars have proper motions less than 25 mas yr^{-1} . As expected, proper motions are smaller for more distant stars; there are some high proper motion stars most of which are located within ~ 200 pc from the Sun. These high proper motion stars are supposed to be high velocity stars. Therefore, we expect that most clusters have proper motions less than 25 mas yr^{-1} . For nearby clusters, we should consider a larger range of proper motions.

3. METHOD

Our process of searching open clusters from the *Gaia* DR2 is divided into two steps. The first step is the visual search for cluster candidates by looking at the multi-dimensional information of *Gaia* DR2 (proper motion, position, and parallax). The second step is the verification of candidate clusters by comparing their CMDs with theoretical isochrones. During the search, physical parameters of clusters such as cluster radius were derived.

3.1. Visual Inspection

We divided the whole sky into 3628 areas for visual inspection of cluster candidates. The size of the search area varied with Galactic latitude (b). Each area was selected to have about 10^5 stars; we set this upper limit for the number of stars in each area to reduce field star contamination and to increase the contrast between field stars and cluster members. Details are given in Table 1.

We first checked the proper motions of stars in each area. The proper motion distribution varies locally and cluster stars are “buried” in field stars (with few exceptions such as the Hyades and Pleiades). We therefore first identify the center of the field star distribution in proper motion space, and then search for off-center

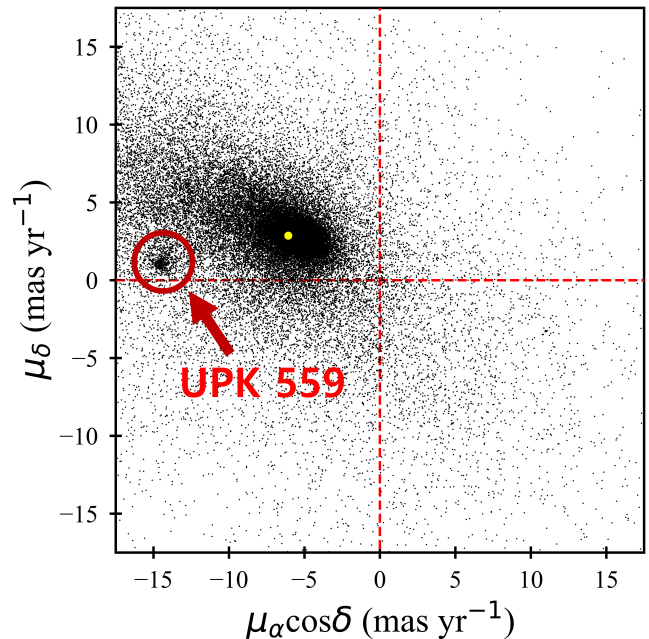


Figure 2. Proper motions of a sample of 47 578 stars located within 2° from $l = 285^\circ$ and $b = 0^\circ$.

local concentrations corresponding to stars of a prospective cluster. Figure 2 shows an example for a set of field stars centered at $\mu_\alpha \cos \delta = -6.08 \text{ mas yr}^{-1}$ and $\mu_\delta = 2.87 \text{ mas yr}^{-1}$.

In a given search area, we first calculated the average proper motion of all stars within 30 mas yr^{-1} from $(0, 0)$. We then re-calculated the average proper motion using all stars located within 30 mas yr^{-1} from the newly found kinematic center; we repeated this procedure until it converged. Our approach reduces the impact of high-proper motion stars. After identification of the kinematic center of the field stars, we visually searched for off-center local concentrations of stars within a radius of 25 mas yr^{-1} . The search radius was obtained by trial and error, guided by the proper motion distribution as a function of parallax shown in Figure 1.

After identifying a candidate cluster in proper motion space, we obtained the (absolute) proper motions of its member stars and determined their spatial distribution in $l - b$ space. In case of clusters with very large proper motions, such as the Hyades cluster, we included stars with proper motions in the range $\pm 150 \text{ mas yr}^{-1}$. We then checked the distribution of their parallaxes for a significant peak caused by a concentration of stars at a certain distance, as required for a physical cluster. If the parallax distribution indeed showed such a peak, we determined the most probable range of parallaxes wherein the clusters stars are likely to be located. After visual inspection of the whole area, we inspected again all the selected cluster candidates to check for ambiguities and duplications. The final number of cluster candidates is 655. The cluster parameters determined by visual inspection were used as initial values for the further analysis described below.

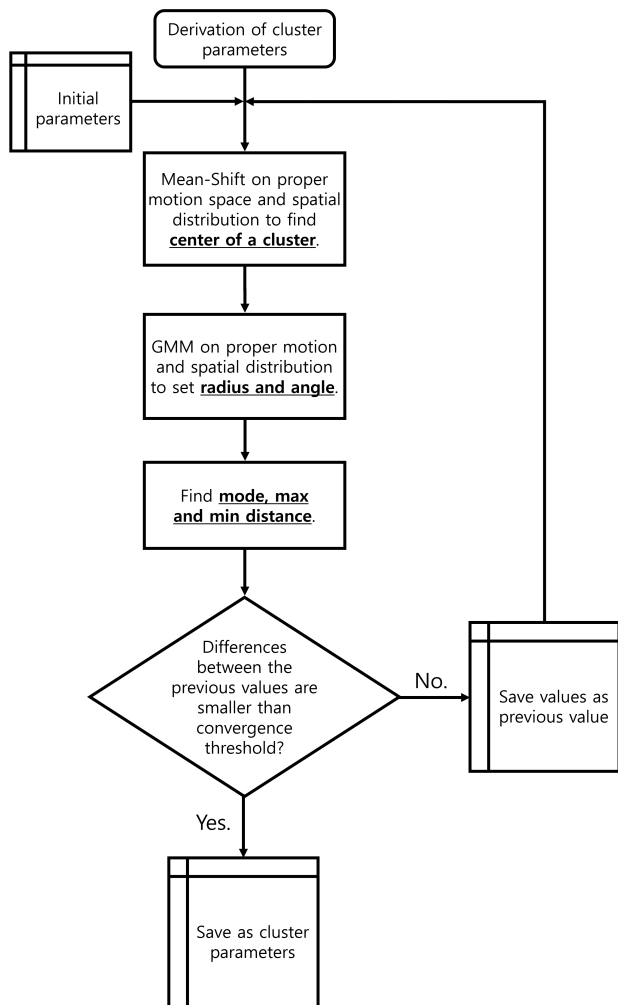


Figure 3. Iterative derivation of the physical parameters of cluster candidates identified from visual inspection.

3.2. Derivation of Cluster Parameters

Since the cluster parameters obtained from visual inspection can only be rough estimates, we further analyzed our cluster candidates using GMM and mean-shift algorithms. For each cluster, we obtained its center and radius in proper motion and $l-b$ space, respectively, its distance from the mode of the distribution of the parallaxes of the cluster stars, and upper and lower limits on the cluster distance, d_{max} and d_{min} .

The covariance and Gaussian center provided by a GMM were used to derive the size and shape of a cluster in terms of axis lengths, position angle (orientation on the sky), and ellipticity. For the GMM analysis, we used the Python library `Scikit-Learn` (Pedregosa et al. 2011). We set the convergence threshold to 0.001 and the mixture component to 1. The mean-shift algorithm was used to find the center of a density distribution. For GMM analysis in $l-b$ space, we weighted the data with the inverse distance from the center. The weights were given by $w_i = (|r_i - 2r|/2r)^p$ where r_i is the distance of a star i from the center, r is the cluster radius and p is

a power index that depends on r . Here, r is defined as the radius in $l-b$ space (r_{GMM}).

We summarize our analysis procedure in Figure 3. We derived the center and radius of a cluster in proper motion and $l-b$ space iteratively using the parameters obtained from the visual inspection as initial values. When we derived the centers of proper motion distributions by mean-shift, we included all stars that are located within the distance range allowed for the cluster. Similarly, in $l-b$ space, we included all stars that satisfy reasonable boundary conditions on proper motion distribution and distance. Some clusters, such as small clusters in the Orion nebula, are located close to each other and have almost the same proper motions. Clusters with similar proper motions happened to be added together by our analysis routines, allowing for an abnormal growth of search radius which hindered a proper determination of the cluster center in proper motion space. We therefore limit the search radius in proper motion space determined by visual inspection. We also limit the search radius in $l-b$ space to the radius determined by visual inspection.

Once cluster parameters in proper motion space were determined from mean-shift analysis, we derived updated values for the cluster parameters in $l-b$ space using the stars that satisfy the criteria for cluster distance and proper motion parameters. We applied ellipse fitting using GMM to determine the shape of the spatial distribution of cluster stars, using the stars that are still compatible with being cluster members after updating the values for distances and range of proper motions. We derived the semi-major axis, semi-minor axis, and the angle between the major axis and the Galactic plane. We applied GMM to the proper motion data, assuming that cluster stars are located within 1σ of the Gaussian model. We defined a radius r_{GMM} as the radius for which the enclosed area is the same as the area of the ellipse derived by GMM. We determined the mode of the distribution of parallaxes by fitting a Gaussian kernel to the parallax distribution of stars that have proper motions allowed for the cluster and are located within the ellipse defined in the spatial distribution. The cluster distance range is given by the full width at half maximum (FWHM) of the Gaussian kernel.

We iterated our procedure until all six parameters – center and radius of proper motion distribution, center and radius of spatial distribution, distance, and angle – converged. In most cases, convergence was achieved when setting the power index p in the weight function to $p = 0.5$ for cluster radii larger than 2° , and to $p = 0.3$ for smaller radii. In some cases, we varied the p values to achieve convergence.

3.3. Color–Magnitude Diagrams

To probe if they actually are physical star clusters, we constructed color–magnitude diagrams for our candidate clusters. We compared each CMD to the metallicity $Z = 0.02$ isochrones of the PARSEC library (Bressan

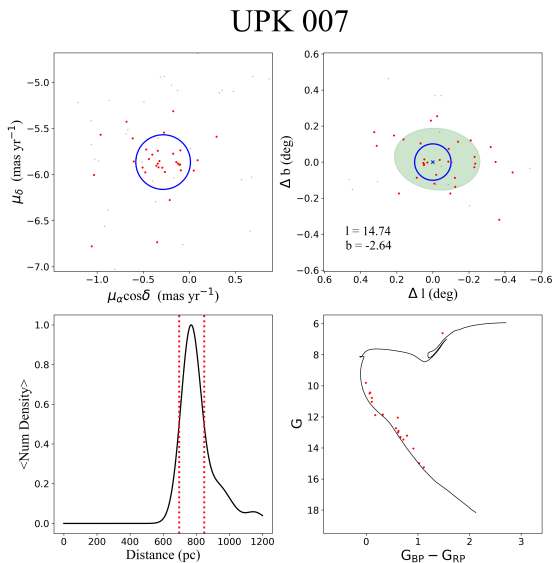


Figure 4. Properties of cluster candidate UPK 007. *Top left:* Proper motion space. *Top right:* $l - b$ space. Blue circles indicate the radii of the stellar distributions. The shaded ellipse marks the spatial distribution found from GMM analysis. *Bottom left:* Distance distribution from fitting a Gaussian kernel. The two vertical dotted lines indicate the distance range adopted for the cluster stars. *Bottom right:* CMD of the cluster stars. The solid line is the best fit isochrone.

et al. 2012), updated for the *Gaia* DR2 passbands² with the photometric calibration of Evans et al. (2018). We used least-squares fitting of isochrones to observed cluster CMDs. The CMDs were corrected for interstellar reddening $E(G_{BP} - G_{RP})$ and the extinction in the G band, A_G , using the extinction values from *Gaia* DR2. For stars with no extinction estimates in *Gaia* DR2, we used the average of the extinction values of the cluster stars. We used the most probable parallax (mode of distribution) as cluster distance. We found that all candidate clusters except of two have CMDs that are well described by theoretical isochrones; we selected the best-fitted isochrones to estimate the cluster ages. Thus, among the 655 visually selected cluster candidates, 653 are physical open clusters (99.7%). The two cluster candidates that failed the validation, UPK 034 and UPK 036, present peculiar CMDs. UPK 034 has a main sequence that covers only $\sim 3\text{mag}$ with a large color spread, and UPK 036 has a main sequence too broad to be considered a cluster main sequence. Both are extremely young ($\sim 6\text{ Myr}$) if they are actual open clusters. Some of our clusters have small numbers of member stars ($N \lesssim 50$) and could be stellar associations or small stellar aggregations, but we nevertheless refer to them as “open clusters”.

3.4. Cross-Matching with Other Catalogs

There are a number of catalogs of open clusters which can be used to check whether the open clusters identified in the present study are new findings or not. We selected the three catalogs DALM, MWSC, and COCD for cross-matching of the 655 visually selected clusters. The total number of clusters listed in the three catalogs is 5755; due to duplications, the number of clusters to be cross-matched with our findings is ~ 3000 . In addition, we cross-matched our sample with the 1229 clusters from DALM by applying UPMASK to the *Gaia* DR2 (Cantat-Gaudin et al. 2018) to check the completeness of our search method. We also cross-matching our clusters with those from recent publications (Röser, Schilbach & Goldman 2016; Castro-Ginard et al. 2018; Cantat-Gaudin et al. 2019).

We considered a candidate cluster to be a known cluster if it has coordinates, proper motions, and a distance that satisfy the following conditions. Firstly, the candidate cluster should be located within the cluster angular radius from the known clusters. That is, $\Delta\theta < r_{cl}$ where $\Delta\theta$ is the angular distance between the candidate cluster and a known cluster and r_{cl} is the angular radius of the candidate cluster measured in $l - b$ space. We used r_{GMM} for r_{cl} . Secondly, the clusters have similar proper motions, meaning here

$$[(\mu_\alpha \cos \delta - \mu_{\alpha_C} \cos \delta_C)^2 + (\mu_\delta - \mu_{\delta_C})^2]^{1/2} < r_{cl(pm)}$$

where $\mu_\alpha \cos \delta$ and μ_δ are the proper motions of the candidate cluster and $\mu_{\alpha_C} \cos \delta_C$ and μ_{δ_C} are those of the known cluster, respectively; $r_{cl(pm)}$ is the radius of the candidate cluster in proper motion space. Thirdly, $d_{min} < d_C < d_{max}$ where d_{min} and d_{max} are the minimum and maximum distance allowed for the candidate cluster and d_C is the distance of the known cluster.

We cross-matched all 655 visually selected cluster candidates with known open clusters as described above. We assigned numeric codes from 0 to 3 for candidate clusters to quantify the degree of agreement. If a candidate cluster did not satisfy any of our three conditions, we assigned code 0. We assigned code 1 to candidate clusters that satisfied only the first condition. Code 2 was assigned to candidate clusters which satisfy the first condition along with either the second or the third condition. If the candidate cluster satisfied all the three conditions, we assigned code 3. Since we wanted to restrict our sample to genuinely unknown clusters, we considered all clusters with a code other than 0 as known. When applying this threshold, we found 207 new open clusters among the 653 clusters that passed the CMD validation test.

4. RESULTS

4.1. Catalog

We summarize all 655 cluster candidates selected from visual inspection of *Gaia* DR2 in an online catalog,³ including the two cluster candidates that failed the CMD

²<http://stev.oapd.inaf.it/cgi-bin/cmd>

³<https://sites.google.com/us/hs.kr/upk>

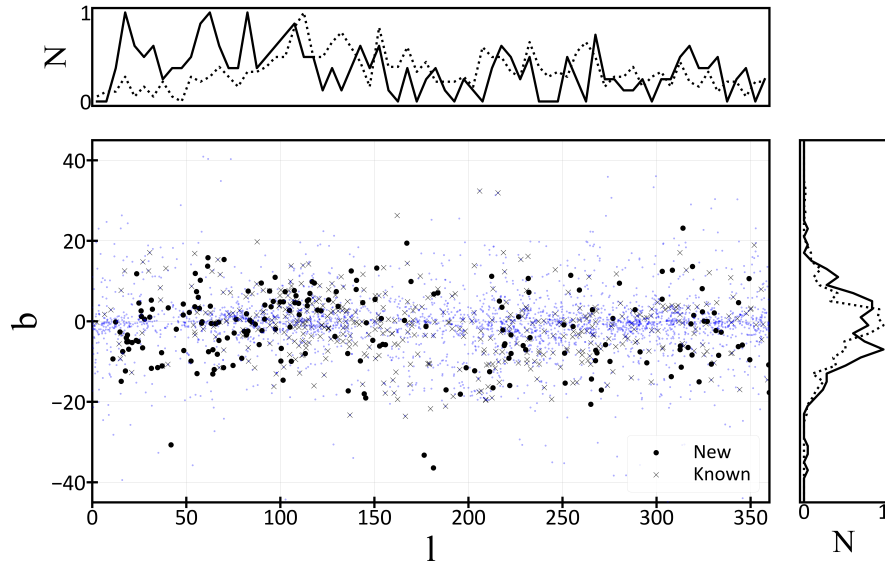


Figure 5. Distribution of open clusters in Galactic coordinates l, b . Newly found clusters, known clusters, and MWSC clusters are plotted as black dots, crosses, and small blue dots, respectively. The frequency distributions of visually identified new and known clusters are shown along the l and b axes, with N being the number; solid lines represent the newly found clusters, dotted lines indicate the known clusters.

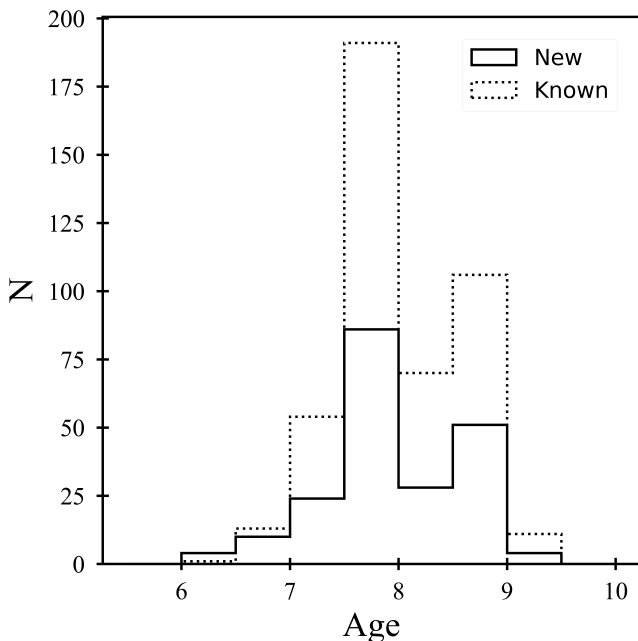


Figure 6. Frequency distribution of cluster ages. Solid lines represent new clusters, dotted lines indicate known clusters.

validation. We provide the cluster data along with figures visualizing the cluster parameters. The catalog provides coordinates, proper motions, and shape parameters derived from GMM analysis. Each figure presents the distribution of cluster stars in proper motion space and $l-b$ space, the distance distribution, and the CMD. An example is given in Figure 4. Distance distributions include all stars identified as cluster members in proper motion space and in $l-b$ space.

We present the basic parameters of the newly discovered 207 open clusters in Table 2. We give Galactic

coordinates, proper motions, parallaxes, r_{GMM} , r_c , numbers of stars within r_{GMM} (N), and cluster ages from the best-fit $Z = 0.02$ PARSEC isochrones. Other parameters such as the magnitude and colors of the brightest cluster star, shape parameters (semi-major and minor axis, ellipticity and position angle θ) are given in the online catalog. The radius r_{GMM} is not the conventional cluster radius but it roughly defines the regions where cluster stars, including escaping stars, are likely to be found.

4.2. Properties of New Clusters

Figure 5 shows the distribution of newly discovered open clusters together with known clusters in Galactic coordinates. The new clusters are less concentrated toward the Galactic plane than the open clusters in MWSC. There are only five clusters at high Galactic latitude with $|b| > 20^\circ$. The absence of high latitude new clusters is consistent with their young to intermediate ages, which suggests that they have not yet migrated far from their birth places in the Galactic disk. There are slightly more new open clusters in $0^\circ < l < 180^\circ$ than in $180^\circ < l < 360^\circ$. There seems to be no significant difference between the Galactic northern sky ($b > 0^\circ$) and southern sky ($b < 0^\circ$).

We plotted the age distribution of the newly found open clusters in Figure 6 together with that of known clusters for comparison. We note that the accuracy of cluster ages is limited because we derived them using a fixed metal abundance of $Z = 0.02$. Nevertheless, we can divide the clusters into three age groups: young ($< 10^8$ yr), intermediate ($10^8 \leq t$ (yr) $< 10^9$), and old ($\geq 10^9$ yr). As shown in Figure 6, the newly found open clusters are mostly young and intermediate-age clusters that have ages of 7.5×10^7 yr $\sim 10^9$ yr. Very young clusters ($< 10^7$ yr) are slightly more abundant than old clusters. The age distribution of newly found

Table 2
Physical parameters of newly discovered open clusters.

ID	l ($^{\circ}$)	b ($^{\circ}$)	μ_{α^*} (mas yr $^{-1}$)	μ_{δ} (mas yr $^{-1}$)	d (pc)	r_{GMM} ($'$) ^a	r_c ($'$) ^b	N^c	log(age)
UPK 4*	10.96	-9.35	-2.03 (0.09)	-6.40 (0.11)	784 (24)	22.48	11.25 (0.07)	37 (89.66)	8.45
UPK 5	12.39	-0.16	0.74 (0.10)	-8.38 (0.17)	550 (16)	23.30	8.26 (0.12)	25 (34.69)	8.00
UPK 7	14.74	-2.64	-0.28 (0.14)	-5.87 (0.08)	769 (22)	12.12	5.99 (0.08)	19 (51.88)	8.40
UPK 12	15.37	-14.92	0.58 (0.10)	-6.61 (0.12)	644 (29)	15.82	10.89 (0.02)	24 (39.24)	7.90
UPK 13	16.18	-7.51	-1.15 (0.10)	-4.12 (0.10)	915 (25)	12.11	2.67 (0.02)	45 (85.00)	7.90
UPK 16	17.63	-12.34	-0.40 (0.18)	-5.14 (0.19)	802 (39)	23.81	6.82 (0.08)	29 (55.16)	7.90
UPK 17	18.11	-4.11	0.90 (0.11)	-7.92 (0.12)	659 (20)	27.44	8.55 (0.08)	39 (83.82)	8.90
UPK 18	18.34	-5.11	3.08 (0.14)	0.87 (0.17)	753 (37)	14.48	6.54 (0.03)	24 (45.65)	8.45
UPK 19	18.70	-3.39	-1.81 (0.28)	-9.33 (0.29)	289 (27)	94.13	44.34 (0.23)	119 (119.00)	8.50
UPK 20	19.24	-5.05	3.32 (0.15)	1.14 (0.14)	472 (23)	44.32	22.11 (0.09)	40 (65.44)	8.80
UPK 21	19.38	-6.93	7.82 (0.10)	0.73 (0.10)	587 (13)	20.98	9.92 (0.03)	22 (53.55)	8.95
UPK 23	21.14	-5.27	-0.90 (0.12)	-2.08 (0.13)	952 (36)	13.04	6.38 (0.14)	19 (52.90)	8.55
UPK 24	23.33	-4.74	-3.75 (0.12)	-9.79 (0.15)	498 (18)	72.33	18.24 (0.97)	32 (44.49)	8.90
UPK 25	23.59	11.81	-0.31 (0.09)	0.19 (0.12)	629 (31)	50.21	24.68 (0.43)	19 (46.17)	8.95
UPK 26	24.44	-5.00	0.08 (0.10)	-4.42 (0.08)	875 (26)	26.23	15.27 (0.16)	42 (78.92)	8.05
UPK 27	24.78	4.54	2.36 (0.10)	-2.14 (0.14)	899 (29)	14.16	5.86 (0.03)	36 (116.70)	9.35
UPK 28	25.98	2.60	0.81 (0.12)	-2.49 (0.13)	882 (33)	13.44	0.98 (0.25)	28 (90.77)	8.90
UPK 29	26.13	1.19	0.45 (0.12)	2.83 (0.11)	656 (13)	13.52	13.38 (0.12)	22 (88.07)	8.75
UPK 31	26.75	-6.59	-0.32 (0.09)	1.21 (0.08)	540 (13)	18.55	10.70 (0.09)	17 (36.62)	7.55
UPK 33	27.78	0.52	-0.13 (0.15)	-10.95 (0.17)	508 (11)	14.29	12.30 (0.11)	16 (33.94)	8.90
UPK 38	30.54	1.04	-1.11 (0.11)	-5.27 (0.10)	572 (7)	8.75	1.52 (0.11)	8 (11.53)	6.45
UPK 39	31.37	5.24	3.29 (0.39)	-8.65 (0.41)	431 (27)	29.77	13.52 (0.07)	62 (117.00)	6.45
UPK 40	31.44	-11.69	0.29 (0.15)	-9.13 (0.17)	641 (31)	58.58	38.19 (0.22)	32 (60.39)	8.75
UPK 41	31.95	3.00	2.51 (0.22)	-8.13 (0.23)	480 (19)	43.23	34.34 (0.16)	61 (115.35)	6.85
UPK 42	34.73	-11.50	-0.46 (0.12)	-5.03 (0.11)	592 (15)	22.54	5.99 (0.03)	41 (77.45)	8.75
UPK 45	36.84	-7.79	-0.62 (0.11)	-2.16 (0.10)	862 (51)	110.95	27.29 (0.24)	179 (335.37)	7.90
UPK 46	37.13	-11.08	0.11 (0.15)	-8.60 (0.17)	680 (25)	27.27	17.18 (0.27)	23 (43.40)	7.90
UPK 50	40.40	3.35	-1.33 (0.11)	-3.79 (0.14)	995 (34)	20.49	14.14 (0.14)	51 (123.74)	8.70
UPK 51	41.87	-30.70	5.06 (0.16)	2.07 (0.11)	567 (22)	34.35	18.46 (0.10)	21 (24.86)	8.00
UPK 52	44.69	-1.96	-0.16 (0.05)	-5.97 (0.10)	818 (28)	12.14	4.24 (0.05)	9 (24.97)	8.05
UPK 53	48.32	1.56	2.44 (0.12)	1.08 (0.09)	591 (13)	26.97	14.93 (0.05)	43 (81.31)	8.90
UPK 54	48.37	4.28	-0.57 (0.12)	-5.88 (0.12)	827 (31)	26.16	14.53 (0.11)	60 (128.62)	7.90
UPK 55	48.66	-7.27	-1.43 (0.11)	-6.86 (0.09)	777 (28)	20.40	7.93 (0.05)	30 (48.86)	7.95
UPK 56	51.57	2.20	-0.07 (0.16)	-6.74 (0.15)	760 (27)	63.41	34.18 (0.17)	87 (186.72)	8.75
UPK 57	52.49	-9.88	-0.45 (0.08)	-3.56 (0.08)	819 (36)	26.31	15.71 (0.12)	14 (22.90)	8.75
UPK 62	54.52	3.61	-0.43 (0.12)	-5.41 (0.08)	895 (40)	16.80	3.41 (0.07)	26 (104.80)	6.75
UPK 64	54.76	11.90	-0.93 (0.11)	-5.03 (0.12)	442 (57)	84.51	30.75 (0.40)	21 (24.89)	8.00
UPK 65	55.40	7.39	-1.86 (0.08)	-3.56 (0.08)	758 (20)	22.06	10.40 (0.04)	23 (43.44)	8.90
UPK 66	55.69	-12.98	0.51 (0.08)	-9.93 (0.10)	669 (13)	21.99	16.40 (0.18)	16 (33.98)	8.10
UPK 70	56.33	5.96	0.33 (0.21)	-5.38 (0.17)	493 (28)	28.30	24.80 (0.13)	27 (37.54)	7.10
UPK 71	56.93	3.20	1.30 (0.28)	-5.48 (0.25)	524 (37)	16.02	5.50 (0.03)	40 (85.27)	6.85
UPK 72	57.42	10.19	-0.68 (0.20)	-4.41 (0.21)	454 (43)	75.81	95.39 (1.27)	57 (67.48)	7.80
UPK 73	58.13	-0.47	0.74 (0.11)	-6.51 (0.13)	634 (22)	11.24	7.87 (0.09)	9 (29.39)	7.25
UPK 74	58.41	-0.11	-0.11 (0.10)	-3.33 (0.10)	571 (38)	26.03	5.12 (0.02)	16 (18.90)	7.95
UPK 77	61.33	13.69	1.08 (0.05)	-4.06 (0.07)	353 (25)	19.72	7.33 (0.25)	7 (8.37)	7.40
UPK 78	61.49	15.81	0.31 (0.28)	-3.52 (0.22)	375 (33)	92.39	133.03 (2.22)	50 (51.13)	7.75
UPK 79	61.81	-7.56	-2.10 (0.14)	-5.47 (0.10)	913 (37)	27.85	12.35 (0.08)	23 (55.80)	7.80
UPK 80	62.75	3.76	1.19 (0.10)	-1.01 (0.09)	876 (49)	35.63	7.09 (0.34)	28 (53.04)	7.90
UPK 82	63.22	-0.54	2.34 (0.11)	-2.13 (0.10)	537 (21)	37.87	25.39 (0.09)	41 (48.48)	7.90
UPK 84	64.07	-13.10	-6.25 (0.07)	-9.25 (0.09)	904 (25)	24.29	13.72 (0.06)	38 (81.56)	8.75
UPK 85	64.12	-7.06	2.12 (0.10)	-1.61 (0.07)	887 (26)	30.12	28.72 (1.15)	11 (24.06)	7.60
UPK 88	64.83	-11.99	10.29 (0.12)	-5.35 (0.19)	293 (19)	64.38	26.84 (0.41)	16 (16.00)	7.80
UPK 90	65.63	-0.63	-0.83 (0.10)	-5.72 (0.08)	793 (32)	13.21	10.56 (0.23)	24 (45.46)	7.65
UPK 91	66.48	-8.18	2.04 (0.13)	-3.97 (0.09)	764 (46)	76.16	31.67 (0.23)	30 (48.98)	8.00
UPK 93	67.19	-0.20	-0.85 (0.10)	-8.28 (0.11)	685 (34)	32.51	7.51 (0.08)	33 (53.88)	8.60

*UPK stands for the names of the authors' institutions: Ulsan Science High School, Pusan National University, Korea Astronomy and Space Science Institute. Numbers in parenthesis are errors.

^aGMM cluster radius.

^bKing profile core radius.

^cNumber of stars within the best-fit ellipse. Numbers in parenthesis are numbers of member stars corrected for the incompleteness due to the magnitude cut at $G = 18$.

Table 2
Continued

ID	l (°)	b (°)	μ_{α^*} (mas yr ⁻¹)	μ_{δ} (mas yr ⁻¹)	d (pc)	r_{GMM} (′) ^a	r_c (′) ^b	N^c	log(age)
UPK 94	67.35	-4.74	2.12 (0.06)	1.06 (0.06)	941 (32)	23.49	9.14 (0.09)	20 (56.01)	7.90
UPK 99	69.80	-11.52	0.27 (0.17)	-7.84 (0.21)	783 (37)	39.05	19.86 (0.74)	20 (32.86)	8.10
UPK 101	70.08	15.36	1.44 (0.33)	-1.63 (0.34)	363 (42)	100.06	112.27 (1.11)	103 (105.30)	7.65
UPK 104	71.82	-4.14	3.67 (0.17)	1.53 (0.17)	836 (35)	40.53	28.16 (0.33)	34 (64.22)	7.95
UPK 108	74.84	-10.97	1.02 (0.11)	-4.72 (0.09)	840 (26)	52.71	13.41 (0.21)	28 (52.95)	7.65
UPK 109	75.43	-2.91	-2.37 (0.08)	-5.67 (0.10)	725 (23)	17.61	0.60 (0.44)	12 (22.67)	7.65
UPK 110	76.38	0.50	2.90 (0.11)	-1.17 (0.08)	857 (15)	30.93	15.10 (0.12)	11 (23.61)	8.65
UPK 113	79.43	-9.19	2.16 (0.08)	-2.34 (0.13)	679 (10)	22.91	8.98 (0.13)	15 (24.51)	7.85
UPK 116	80.78	-2.48	3.28 (0.08)	-2.94 (0.06)	435 (19)	31.69	11.21 (0.06)	14 (14.32)	7.75
UPK 118	81.92	-3.39	-1.65 (0.08)	-3.50 (0.09)	940 (40)	73.88	19.62 (0.10)	38 (92.76)	8.90
UPK 119	81.99	1.87	-0.65 (0.06)	-2.00 (0.07)	769 (11)	16.50	11.93 (1.30)	18 (43.67)	8.75
UPK 120	82.12	-3.14	2.76 (0.16)	-1.44 (0.15)	666 (20)	38.40	6.37 (0.09)	22 (47.22)	7.75
UPK 121	82.77	-2.43	0.57 (0.15)	-1.87 (0.12)	951 (52)	48.17	27.03 (0.18)	43 (139.39)	8.95
UPK 122	82.86	7.50	-1.34 (0.07)	-9.26 (0.04)	900 (25)	36.29	51.93 (5.82)	13 (34.41)	9.40
UPK 126	83.78	0.27	-1.46 (0.16)	-1.89 (0.18)	823 (36)	9.61	1.90 (0.06)	15 (41.32)	6.75
UPK 127	84.82	-0.17	-1.29 (0.39)	-3.08 (0.42)	796 (48)	26.37	12.74 (0.03)	161 (439.08)	6.25
UPK 131	86.66	-0.73	2.83 (0.10)	-1.09 (0.07)	976 (25)	19.63	8.44 (0.05)	24 (77.61)	8.75
UPK 136	88.73	-5.79	-0.03 (0.16)	-0.60 (0.12)	643 (35)	50.28	35.17 (0.35)	42 (58.40)	7.85
UPK 137	89.84	9.50	-2.34 (0.10)	-6.04 (0.09)	838 (28)	22.02	9.22 (0.02)	19 (46.25)	7.50
UPK 138	90.21	-2.32	-0.41 (0.15)	-1.78 (0.13)	681 (12)	10.73	1.63 (0.18)	11 (35.66)	6.50
UPK 143	91.62	0.55	1.07 (0.12)	-2.46 (0.11)	861 (26)	50.42	9.34 (0.07)	65 (207.93)	8.85
UPK 144	91.74	4.04	1.17 (0.38)	-3.41 (0.26)	557 (29)	20.50	6.17 (0.05)	27 (66.34)	6.45
UPK 147	94.25	7.51	-2.39 (0.19)	-4.83 (0.23)	883 (35)	106.71	98.88 (0.70)	188 (448.76)	7.25
UPK 150	95.06	3.62	-4.25 (0.09)	-3.99 (0.09)	980 (33)	48.73	15.75 (0.06)	40 (129.11)	7.20
UPK 152	96.18	4.94	3.73 (0.10)	-1.17 (0.12)	739 (35)	47.42	13.29 (0.20)	19 (46.38)	9.00
UPK 155	97.22	10.93	-2.24 (0.09)	-3.86 (0.15)	887 (23)	45.48	10.40 (0.13)	23 (56.15)	7.55
UPK 156	97.32	-1.95	-0.32 (0.10)	-1.91 (0.08)	902 (27)	26.36	10.72 (0.15)	14 (26.31)	7.90
UPK 160	98.40	15.02	3.68 (0.21)	0.29 (0.18)	480 (15)	29.30	2.03 (0.20)	14 (22.89)	6.70
UPK 164	99.92	4.82	-1.46 (0.18)	-3.26 (0.17)	933 (45)	71.26	16.23 (0.16)	124 (339.67)	7.25
UPK 166	100.27	-9.88	-0.92 (0.12)	-3.26 (0.17)	651 (27)	75.77	17.49 (0.12)	131 (181.84)	7.60
UPK 167	100.48	-6.74	1.56 (0.17)	-0.09 (0.16)	545 (33)	101.05	38.98 (0.17)	89 (105.17)	8.00
UPK 168	101.43	-14.64	-0.53 (0.13)	-3.95 (0.13)	596 (21)	72.94	16.40 (0.13)	99 (137.16)	7.65
UPK 169	101.63	4.84	-1.95 (0.15)	-2.36 (0.16)	842 (30)	52.97	10.24 (0.10)	64 (152.85)	7.10
UPK 172	102.55	7.35	-2.06 (0.12)	-3.04 (0.10)	909 (34)	17.14	3.74 (0.04)	35 (84.81)	7.15
UPK 178	104.86	2.71	-4.34 (0.15)	-3.36 (0.14)	949 (21)	5.73	1.53 (0.03)	15 (48.42)	8.50
UPK 180	105.11	-1.44	-0.61 (0.17)	0.21 (0.16)	832 (38)	45.13	18.83 (0.08)	40 (75.64)	8.55
UPK 185	105.82	-9.95	2.66 (0.16)	-1.93 (0.17)	552 (23)	31.02	5.25 (0.03)	83 (98.27)	7.95
UPK 189	107.39	7.64	-2.65 (0.10)	-3.32 (0.11)	1001 (40)	44.04	44.48 (0.41)	31 (86.50)	7.20
UPK 191	107.68	4.61	-1.04 (0.16)	-1.87 (0.17)	874 (37)	37.11	0.02 (0.00)	34 (107.73)	6.90
UPK 194	108.29	6.36	-0.76 (0.31)	-3.09 (0.33)	924 (33)	25.37	8.27 (0.02)	92 (250.28)	7.35
UPK 198	109.68	4.45	-4.90 (0.10)	-2.14 (0.11)	844 (26)	50.72	6.00 (0.07)	27 (74.92)	8.60
UPK 201	109.99	1.64	-3.95 (0.16)	-3.37 (0.09)	919 (15)	16.20	1.80 (0.22)	18 (58.21)	6.60
UPK 214	113.24	-8.02	0.79 (0.21)	-0.72 (0.21)	810 (46)	95.14	53.33 (0.23)	111 (180.78)	8.75
UPK 219	114.27	3.86	-1.72 (0.06)	-2.48 (0.07)	801 (19)	23.39	6.11 (0.11)	15 (32.24)	8.90
UPK 220	114.35	5.10	-2.41 (0.13)	-2.59 (0.12)	967 (28)	23.57	6.15 (0.04)	102 (326.29)	8.75
UPK 224	114.99	5.35	-1.41 (0.11)	-0.10 (0.12)	779 (21)	20.33	4.60 (0.09)	30 (97.25)	6.85
UPK 226	115.70	6.93	-1.55 (0.09)	-3.13 (0.07)	861 (14)	26.66	13.95 (0.13)	25 (60.65)	8.80
UPK 230	116.88	9.85	4.90 (0.10)	-0.79 (0.12)	535 (17)	31.45	24.66 (0.37)	19 (26.29)	8.35
UPK 233	118.06	9.50	6.89 (0.18)	0.69 (0.19)	493 (13)	48.50	22.95 (0.33)	18 (25.00)	7.90
UPK 237	119.80	2.81	-0.59 (0.15)	-3.75 (0.17)	735 (21)	25.59	5.26 (0.04)	53 (112.56)	7.65
UPK 241	121.62	2.60	0.17 (0.13)	-0.20 (0.10)	949 (25)	29.81	13.53 (0.05)	27 (87.31)	8.90
UPK 252	125.62	5.31	-1.46 (0.14)	-0.85 (0.16)	858 (47)	103.73	20.87 (0.18)	47 (130.41)	7.40
UPK 260	128.99	-3.75	2.66 (0.12)	-1.86 (0.14)	825 (42)	75.73	31.92 (0.36)	54 (101.83)	7.90
UPK 262	129.73	7.38	-1.97 (0.07)	0.77 (0.08)	825 (32)	52.06	44.28 (0.29)	14 (38.57)	8.50
UPK 265	130.67	3.73	-0.51 (0.09)	-0.37 (0.11)	864 (32)	35.01	12.74 (0.08)	40 (96.93)	8.60

*UPK stands for the names of the authors' institutions: Ulsan Science High School, Pusan National University, Korea Astronomy and Space Science Institute. Numbers in parenthesis are errors.

^aGMM cluster radius.

^bKing profile core radius.

^cNumber of stars within the best-fit ellipse. Numbers in parenthesis are numbers of member stars corrected for the incompleteness due to the magnitude cut at $G = 18$.

Table 2
Continued

ID	l (°)	b (°)	μ_{α^*} (mas yr ⁻¹)	μ_{δ} (mas yr ⁻¹)	d (pc)	r_{GMM} (′) ^a	r_c (′) ^b	N^c	log(age)
UPK 281	135.79	-8.00	-4.07 (0.16)	0.39 (0.13)	624 (59)	107.05	41.18 (0.50)	38 (52.77)	8.10
UPK 282	136.05	-17.30	-2.79 (0.12)	-3.19 (0.12)	807 (40)	19.62	7.71 (0.05)	22 (42.17)	7.90
UPK 287	137.67	12.52	-2.38 (0.27)	-3.46 (0.26)	630 (75)	117.96	65.11 (0.76)	52 (97.21)	8.45
UPK 292	140.30	7.91	0.23 (0.17)	-8.12 (0.19)	444 (33)	66.80	9.92 (0.17)	28 (45.81)	8.80
UPK 294	140.45	10.18	-1.27 (0.13)	2.25 (0.18)	746 (17)	50.23	59.44 (0.86)	27 (51.05)	8.95
UPK 296	142.50	-9.83	1.97 (0.27)	-6.75 (0.31)	538 (49)	66.41	23.15 (0.11)	49 (57.94)	7.95
UPK 300	143.78	4.64	0.25 (0.13)	-0.75 (0.10)	962 (42)	35.87	15.55 (0.08)	21 (57.85)	8.60
UPK 303	144.56	-18.03	18.25 (0.38)	-24.33 (0.49)	212 (8)	149.18	32.94 (0.68)	33 (33.00)	7.95
UPK 305	145.35	-19.04	2.96 (0.13)	-6.50 (0.10)	411 (31)	92.07	25.93 (0.43)	32 (32.72)	7.95
UPK 307	145.71	-0.37	-2.13 (0.18)	-1.82 (0.17)	893 (41)	71.62	18.20 (0.16)	54 (128.96)	7.25
UPK 310	149.14	-4.72	-2.66 (0.07)	0.61 (0.11)	620 (62)	79.73	0.06 (0.00)	14 (19.43)	7.75
UPK 312	150.30	5.44	0.20 (0.07)	-0.73 (0.07)	702 (22)	49.58	0.02 (0.00)	23 (44.09)	8.90
UPK 317	151.23	13.22	-1.11 (0.19)	-1.46 (0.17)	900 (52)	77.98	12.95 (0.43)	42 (89.94)	7.60
UPK 322	152.74	-6.13	-1.39 (0.15)	-2.99 (0.15)	955 (26)	26.83	9.49 (0.05)	60 (127.43)	7.55
UPK 325	153.66	0.68	-1.55 (0.08)	-2.30 (0.08)	762 (28)	17.30	17.35 (0.15)	11 (38.59)	7.95
UPK 326	154.42	-5.74	-2.16 (0.30)	0.10 (0.34)	646 (50)	77.08	49.70 (0.42)	40 (65.39)	8.95
UPK 333	155.85	-5.81	2.53 (0.14)	-6.47 (0.13)	723 (41)	36.65	12.76 (0.08)	30 (56.61)	8.80
UPK 347	165.93	0.22	-0.46 (0.12)	-3.70 (0.06)	917 (30)	35.90	3.93 (0.25)	19 (35.89)	7.90
UPK 350	167.21	19.42	-4.88 (0.17)	-6.39 (0.17)	444 (23)	88.17	30.22 (0.13)	37 (37.83)	8.00
UPK 357	169.46	9.90	-0.33 (0.12)	-1.21 (0.11)	716 (59)	162.52	32.63 (0.36)	36 (58.51)	8.20
UPK 367	176.45	-33.27	24.93 (0.67)	-24.34 (0.52)	162 (46)	294.39	123.78 (0.65)	42 (42.00)	7.95
UPK 369	177.42	-1.28	0.08 (0.06)	-2.89 (0.08)	731 (25)	43.64	14.43 (0.14)	18 (38.69)	8.85
UPK 378	181.37	-36.43	21.48 (0.31)	-13.79 (0.33)	182 (6)	71.27	10.56 (0.29)	13 (13.00)	7.90
UPK 379	181.60	6.79	-0.97 (0.10)	-4.29 (0.08)	765 (38)	54.68	10.06 (0.11)	22 (41.52)	8.80
UPK 381	183.70	7.05	0.48 (0.08)	-2.96 (0.08)	708 (24)	53.72	17.35 (0.06)	28 (53.04)	8.00
UPK 385	188.05	-17.04	1.87 (0.34)	-3.52 (0.28)	320 (34)	46.18	10.05 (0.15)	38 (38.87)	7.00
UPK 394	195.66	-18.11	-0.52 (0.10)	-2.03 (0.10)	802 (24)	25.53	7.95 (0.06)	27 (51.05)	7.90
UPK 398	198.75	-11.55	-3.34 (0.18)	-1.76 (0.18)	452 (32)	39.66	9.45 (0.06)	40 (55.62)	7.10
UPK 402	203.26	-12.30	-1.15 (0.31)	-1.96 (0.28)	429 (35)	21.12	10.45 (0.04)	43 (71.03)	6.85
UPK 416	211.24	-12.52	-1.26 (0.12)	1.48 (0.15)	871 (48)	99.53	23.30 (0.25)	34 (73.07)	7.90
UPK 418	212.31	11.18	-2.68 (0.09)	-1.60 (0.10)	828 (28)	32.25	9.75 (0.08)	17 (27.85)	7.95
UPK 422	213.03	-16.53	0.25 (0.21)	-0.60 (0.22)	304 (22)	63.58	23.01 (0.08)	71 (71.00)	7.30
UPK 429	216.44	5.03	-2.01 (0.14)	0.07 (0.12)	865 (38)	41.86	7.57 (0.12)	76 (143.42)	7.95
UPK 431	217.79	3.49	-2.44 (0.10)	0.77 (0.11)	729 (33)	54.19	13.95 (0.12)	55 (89.39)	8.70
UPK 433	218.28	-2.15	-0.78 (0.13)	-2.55 (0.11)	780 (29)	43.06	7.61 (0.23)	51 (83.38)	7.90
UPK 436	219.00	-6.02	-4.10 (0.14)	0.66 (0.17)	842 (50)	52.09	25.33 (0.13)	67 (126.34)	7.30
UPK 438	219.35	-5.60	-6.59 (0.44)	2.68 (0.37)	449 (60)	95.65	29.13 (0.16)	52 (53.17)	7.80
UPK 442	221.51	-9.17	-2.54 (0.18)	-1.32 (0.17)	640 (45)	88.53	43.49 (0.32)	55 (76.20)	7.70
UPK 445	221.93	-15.95	-2.41 (0.39)	1.45 (0.33)	667 (48)	84.12	25.18 (0.24)	131 (213.35)	7.10
UPK 447	222.57	-3.38	-3.60 (0.08)	0.41 (0.11)	962 (32)	41.40	23.51 (0.06)	30 (57.06)	7.65
UPK 448	222.64	-8.00	-2.61 (0.17)	0.73 (0.17)	900 (42)	44.21	30.58 (0.76)	37 (69.82)	7.90
UPK 452	226.65	1.13	-5.80 (0.08)	3.19 (0.08)	623 (10)	23.99	5.68 (0.09)	9 (25.11)	7.60
UPK 456	229.07	-6.03	-7.62 (0.21)	0.18 (0.17)	506 (41)	100.85	33.68 (0.10)	31 (36.72)	7.95
UPK 457	230.41	-7.05	-3.81 (0.10)	5.14 (0.10)	949 (33)	23.73	6.24 (0.08)	16 (40.86)	7.40
UPK 467	231.78	10.65	-6.99 (0.12)	-1.72 (0.11)	579 (26)	49.73	16.03 (0.09)	49 (68.08)	8.20
UPK 468	232.13	7.20	-1.58 (0.08)	0.10 (0.11)	871 (39)	22.52	4.06 (0.22)	22 (36.14)	8.20
UPK 470	232.73	-4.05	-4.81 (0.11)	4.23 (0.10)	999 (36)	44.70	8.02 (0.10)	55 (104.00)	7.50
UPK 492	250.73	-0.88	-7.43 (0.10)	5.39 (0.07)	713 (26)	42.72	0.02 (0.00)	17 (23.50)	7.90
UPK 494	251.06	-7.92	-5.35 (0.08)	5.25 (0.10)	881 (38)	53.37	18.51 (0.16)	19 (31.74)	7.75
UPK 495	251.37	-15.37	-2.42 (0.14)	5.67 (0.17)	664 (42)	83.78	24.62 (0.31)	36 (58.51)	8.45
UPK 499	254.36	11.42	-6.75 (0.19)	2.67 (0.17)	1001 (70)	110.31	113.82 (1.36)	106 (199.17)	7.90
UPK 502	255.60	-1.29	-8.08 (0.17)	5.61 (0.17)	699 (19)	15.96	3.76 (0.06)	22 (35.99)	7.85
UPK 508	258.93	7.76	-10.58 (0.09)	6.25 (0.09)	830 (20)	26.33	2.98 (0.10)	26 (63.08)	8.60
UPK 524	265.00	-20.62	-2.77 (0.19)	8.81 (0.25)	554 (30)	77.75	38.60 (0.22)	40 (47.29)	8.00
UPK 526	265.35	-14.34	-7.98 (0.19)	7.42 (0.14)	575 (23)	86.20	27.79 (0.23)	30 (41.63)	7.30

*UPK stands for the names of the authors' institutions: Ulsan Science High School, Pusan National University, Korea Astronomy and Space Science Institute. Numbers in parenthesis are errors.

^aGMM cluster radius.

^bKing profile core radius.

^cNumber of stars within the best-fit ellipse. Numbers in parenthesis are numbers of member stars corrected for the incompleteness due to the magnitude cut at $G = 18$.

Table 2
Continued

ID	l ($^{\circ}$)	b ($^{\circ}$)	μ_{α^*} (mas yr $^{-1}$)	μ_{δ} (mas yr $^{-1}$)	d (pc)	r_{GMM} ($'$) ^a	r_c ($'$) ^b	N^c	log(age)
UPK 528	265.90	2.90	-7.69 (0.13)	1.89 (0.13)	953 (41)	32.23	2.37 (0.20)	51 (96.33)	7.90
UPK 533	267.52	-9.78	-7.03 (0.17)	2.57 (0.16)	348 (24)	76.95	18.48 (0.34)	23 (23.52)	7.90
UPK 535	267.66	-7.22	-13.08 (0.36)	3.25 (0.22)	319 (12)	81.14	63.64 (0.68)	72 (72.00)	7.65
UPK 537	268.29	-7.86	-6.69 (0.17)	7.58 (0.18)	603 (37)	60.17	29.99 (0.28)	42 (68.66)	7.60
UPK 540	270.63	-17.08	-4.82 (0.22)	7.66 (0.19)	372 (23)	74.66	33.24 (0.04)	44 (44.99)	7.50
UPK 542	272.86	-5.81	-4.87 (0.07)	2.56 (0.12)	835 (30)	50.70	21.67 (0.05)	19 (35.93)	8.80
UPK 545	275.19	-9.96	-8.74 (0.33)	2.77 (0.32)	331 (28)	99.33	23.37 (0.16)	142 (142.00)	7.95
UPK 549	276.79	0.70	-1.69 (0.13)	-0.43 (0.11)	1010 (25)	24.95	6.96 (0.04)	104 (222.72)	9.05
UPK 552	280.22	9.47	-22.45 (0.38)	6.31 (0.32)	345 (61)	85.98	17.85 (0.05)	43 (43.00)	7.95
UPK 562	288.58	2.88	-11.67 (0.15)	4.85 (0.16)	816 (29)	44.23	12.06 (0.09)	45 (73.57)	7.90
UPK 567	291.21	-7.60	-6.37 (0.11)	0.11 (0.14)	638 (24)	63.52	12.18 (0.08)	54 (74.96)	8.70
UPK 569	294.78	-10.32	-25.75 (0.63)	-1.05 (0.81)	252 (26)	88.53	42.96 (0.32)	63 (63.00)	7.55
UPK 578	302.97	5.49	-12.93 (0.08)	-4.67 (0.08)	942 (24)	16.03	3.99 (0.02)	23 (92.38)	8.85
UPK 579	303.01	12.41	-10.73 (0.21)	-3.20 (0.18)	717 (39)	101.05	36.49 (0.17)	76 (105.54)	7.90
UPK 585	307.83	-13.76	-6.80 (0.15)	-5.55 (0.16)	710 (44)	38.48	3.84 (0.26)	27 (44.36)	7.90
UPK 587	308.37	12.70	-8.82 (0.21)	-2.60 (0.21)	891 (41)	73.13	21.89 (0.17)	78 (147.19)	7.95
UPK 594	312.49	-7.05	-1.98 (0.20)	-3.16 (0.20)	939 (43)	69.82	22.84 (0.08)	78 (147.33)	7.90
UPK 595	312.66	-6.12	-5.93 (0.14)	-3.92 (0.18)	875 (74)	67.38	12.59 (0.20)	56 (105.89)	8.80
UPK 596	313.12	-11.39	-4.40 (0.15)	-3.70 (0.19)	711 (49)	76.17	19.08 (0.12)	36 (58.90)	8.00
UPK 599	314.03	23.16	-9.95 (0.27)	0.30 (0.22)	670 (38)	74.25	18.30 (0.10)	56 (91.44)	7.30
UPK 602	316.71	-6.50	-1.32 (0.21)	-3.94 (0.26)	886 (54)	93.77	65.51 (0.80)	131 (245.44)	7.90
UPK 604	318.25	-0.64	-4.52 (0.11)	-3.62 (0.11)	761 (31)	32.32	7.14 (0.10)	31 (75.21)	7.15
UPK 605	318.84	-8.37	-3.63 (0.08)	-4.28 (0.08)	736 (17)	22.23	3.73 (0.09)	34 (55.70)	7.85
UPK 606	319.09	13.62	-20.26 (0.40)	-16.80 (0.41)	170 (15)	81.53	17.63 (0.11)	40 (40.00)	7.10
UPK 607	319.74	1.46	-4.26 (0.23)	-3.24 (0.23)	900 (65)	20.58	4.30 (0.06)	47 (114.21)	7.10
UPK 612	322.59	-15.03	-13.27 (0.92)	-12.06 (0.91)	241 (32)	181.72	79.39 (0.23)	181 (181.00)	8.00
UPK 613	324.23	8.11	-4.54 (0.09)	-3.63 (0.10)	871 (32)	19.00	8.20 (0.07)	18 (43.94)	7.85
UPK 614	324.35	2.36	-1.84 (0.10)	-4.48 (0.07)	889 (29)	24.72	4.01 (0.14)	27 (51.15)	7.95
UPK 617	325.25	0.04	-2.71 (0.13)	-5.30 (0.10)	723 (17)	21.41	5.47 (0.02)	44 (72.08)	7.90
UPK 621	326.93	-0.03	-2.57 (0.29)	-3.08 (0.24)	866 (44)	37.68	6.88 (0.28)	87 (164.05)	8.80
UPK 624	329.08	-10.65	-1.44 (0.25)	-14.33 (0.28)	325 (38)	52.10	17.34 (0.13)	32 (32.00)	7.65
UPK 626	330.69	2.09	-7.30 (0.22)	-5.67 (0.19)	510 (34)	40.76	9.51 (0.04)	38 (52.79)	8.20
UPK 627	331.53	-2.29	-2.44 (0.16)	-10.06 (0.15)	530 (25)	44.69	13.57 (0.11)	34 (40.24)	8.00
UPK 629	332.99	-8.44	0.80 (0.10)	-3.80 (0.11)	922 (34)	40.86	19.18 (0.18)	33 (70.92)	7.90
UPK 630	334.33	-2.71	-1.75 (0.09)	-2.30 (0.08)	931 (27)	12.32	4.04 (0.01)	32 (89.29)	7.85
UPK 639	343.41	-6.29	1.15 (0.28)	-9.30 (0.29)	707 (59)	118.23	62.90 (0.82)	135 (187.40)	8.90
UPK 640	343.55	4.64	-11.89 (0.49)	-21.15 (0.47)	177 (7)	116.15	41.19 (0.10)	340 (340.00)	7.50
UPK 642	345.57	-5.90	2.31 (0.11)	-4.29 (0.12)	950 (46)	42.53	21.02 (0.69)	34 (64.11)	8.00
UPK 644	349.15	10.62	-3.94 (0.16)	-3.46 (0.13)	742 (29)	37.99	6.87 (0.11)	42 (68.61)	7.95
UPK 645	349.54	-9.55	2.76 (0.13)	-2.85 (0.12)	683 (27)	26.87	8.13 (0.03)	39 (63.89)	7.95
UPK 654	359.58	-10.83	1.13 (0.20)	-8.65 (0.17)	503 (29)	33.74	11.02 (0.05)	49 (58.08)	8.00
UPK 655	359.89	-17.71	4.48 (0.77)	-27.20 (0.82)	153 (5)	26.24	9.83 (0.06)	35 (35.00)	7.10

*UPK stands for the names of the authors' institutions: Ulsan Science High School, Pusan National University, Korea Astronomy and Space Science Institute. Numbers in parenthesis are errors.

^aGMM cluster radius.

^bKing profile core radius.

^cNumber of stars within the best-fit ellipse. Numbers in parenthesis are numbers of member stars corrected for the incompleteness due to the magnitude cut at $G = 18$.

clusters is similar to that of the known clusters. The age distribution we find is similar to that observed in known clusters by Piskunov et al. (2018). The small number of old open clusters among the newly found open clusters is due to the fact that well defined old open clusters are easy to find because most of them are populous and located at high Galactic latitudes. Moreover, old open clusters with small numbers of member stars are prone to dissolution by dynamical evolution which drives mass segregation and evaporation of low mass stars (Michie

1964; Terlevich 1987; Friel 1995).

Figure 7 shows the surface density profile of the newly discovered cluster UPK 007, derived by counting the number of stars in concentric annuli and division by the annulus area. We plotted five profiles which were derived using different sets of aperture interval and width. We set the width of the first aperture to half of r_{GMM} and decrease the width with increasing distance from the center. The typical width of the outermost aperture is one tenth of r_{GMM} which is assumed to be

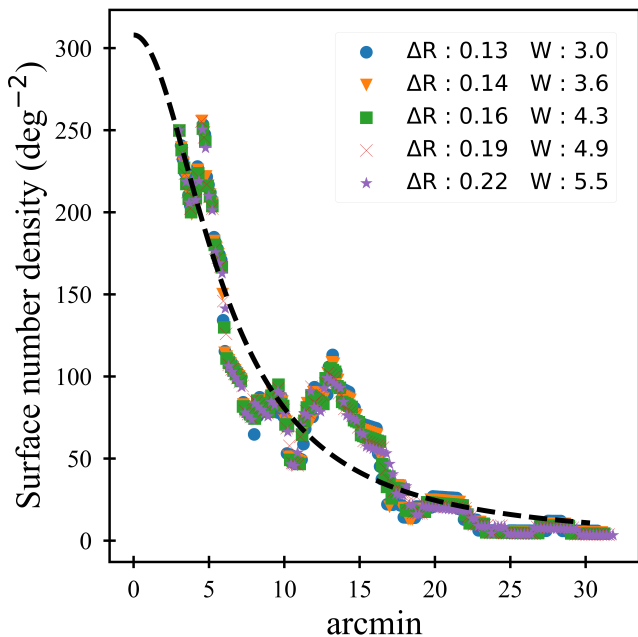


Figure 7. Surface density profiles of UPK 007. Profiles denoted by different symbols are extracted using different sets of aperture parameters given in the upper right corner; ΔR is the aperture interval and W is the width of the outermost aperture. The King model derived from the mean values of f_0 and r_c from the five profiles is indicated by the solid line.

the cluster radius. The averaged surface density profile was fitted with the King model (King 1966)

$$f(r) = \frac{f(0)}{1 + (r/r_c)^2} + f_b$$

where $f(0)$ is the central surface density, r_c is the core radius, and f_b is the constant background surface density. We present the frequency distribution of core radii (r_c) of new open clusters in Figure 8 together with that of the known open clusters. We estimated the errors in r_c from the errors caused by the uncertainty in the derivation of the surface density profile. We derived five values of r_c and calculated the mean and standard deviation. We considered the standard deviation of the five measures of r_c to be the error in r_c .

As shown in Figure 8, most of the new clusters have r_c smaller than ~ 4 pc with the average value being 3.7 pc. This is about twice as much as the mean value of 1.8 pc of the clusters in MWSC. The large mean r_c of the new clusters seems to be due to a more complete census of member stars. The *Gaia* proper motions make it possible to catch escaping cluster stars which are located close to the tidal radius, which is about the same as r_{GMM} . As shown in Figure 9, there is a good correlation between r_{GMM} and r_c . The size of r_c is about 4 times smaller than r_{GMM} . We over plotted the density of clusters in r_{GMM} - r_c space to see the number distribution together.

Figure 10 shows the distribution of the number of members within r_{GMM} for our 653 detected open

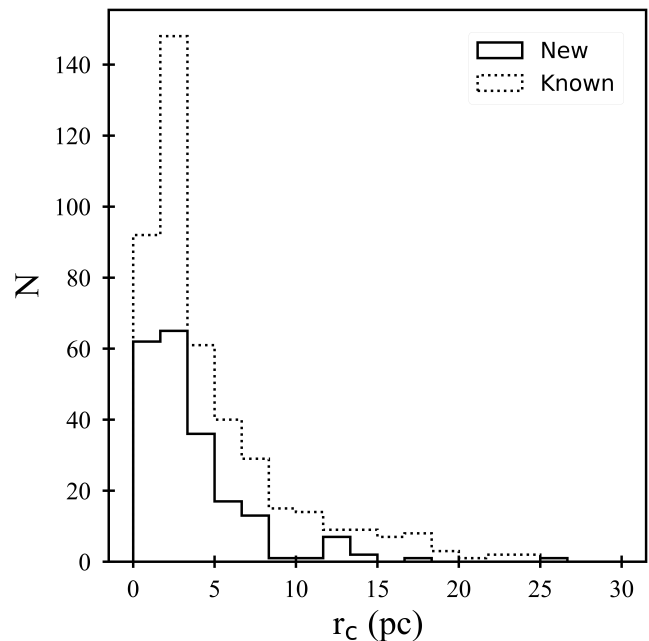


Figure 8. Frequency distribution of core radii (r_c) of our 653 open clusters. Solid lines represent the 207 newly discovered clusters, dotted lines represent the 453 known clusters.

clusters, corrected for the incompleteness caused by the magnitude cut at $G = 18$. We used the luminosity functions derived from $Z = 0.02$ PARSEC isochrones (Bressan et al. 2012) which assumed the initial mass function of Kroupa (2001, 2002). The correction factor for the incompleteness f is given by

$$f = \frac{\int_{M_{l,model}}^{M_{u,obs}} \Psi(M) dM}{\int_{M_{l,obs}}^{M_{u,obs}} \Psi(M) dM}$$

where $\Psi(M)$ is the luminosity function of the model cluster and $M_{l,model}$ is the lower limiting magnitude of the model cluster. $M_{l,obs}$ and $M_{u,obs}$ are the lower and upper limiting magnitudes of the observed cluster, respectively. The majority (75%) of newly discovered clusters have less than 50 member stars while only 27% of the known clusters have that few members. This is the reason why they remained undetected. The most populous cluster (UPK 638) has 340 stars. The second-most populous cluster (UPK 045) has a very elongated shape and is located at ~ 900 pc. As shown in Figure 11, some clusters have unusually small numbers of member stars given their radii.

5. SUMMARY AND DISCUSSION

We visually found 655 clusters within 1 kpc from the Sun using the astrometric (proper motion, position, parallax) and photometric data of *Gaia* DR2, exploiting the fact that stars bound together in a cluster have similar proper motions and are spatially clustered. We used only stars brighter than $G=18$ to reduce contamination by field

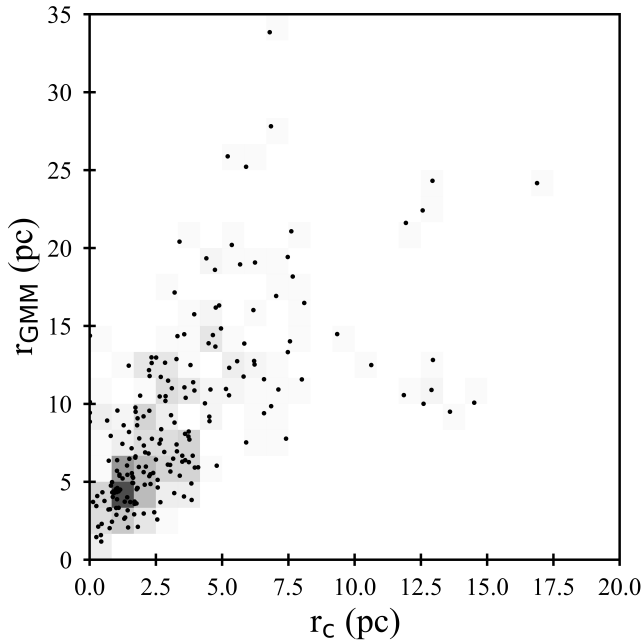


Figure 9. Comparison of r_c and r_{GMM} for our 207 new open clusters.

stars caused by the fact that measurement errors increase as the brightness of stars decreases.

We applied mean-shift and GMM analysis to identify clusters in proper motion space and spatial distributions. We derived cluster parameters such as the radii in which cluster stars are located in proper motion space (r_{PM}) and $l-b$ space (r_{GMM}) iteratively. We validated cluster candidates by comparing their CMDs with PARSEC $Z = 0.02$ isochrones, which resulted in confirmation of 653 open clusters from the 655 visually identified cluster candidates. We cross-matched all 655 visually identified cluster candidates with previous catalogs. We found 207 new open clusters among the 653 clusters that pass CMD validation. Some of the new open clusters might actually be associations or small stellar aggregations given the small numbers of member stars.

We present the physical parameters of the 207 new clusters in a catalog that provides Galactic coordinates, mean proper motions, parallaxes, r_{GMM} , r_c , numbers of member stars within r_{GMM} , and ages. We also present properties of our 655 visually selected cluster candidates in an online catalog. The newly found open clusters have physical properties similar to those of known clusters, with some notable exceptions. Their mean core radius (r_c) is 3.7 pc while that of known clusters is 1.8 pc. Since known clusters are generally more populous than the new open clusters, it is apparent that the known open clusters were the ones that could be found more easily. The majority of newly found clusters have less than ~ 50 member stars with the largest one having 340. The large core radii and small numbers of member stars of the new clusters are likely due to dynamical evolution that leads to the evaporation of low mass stars from

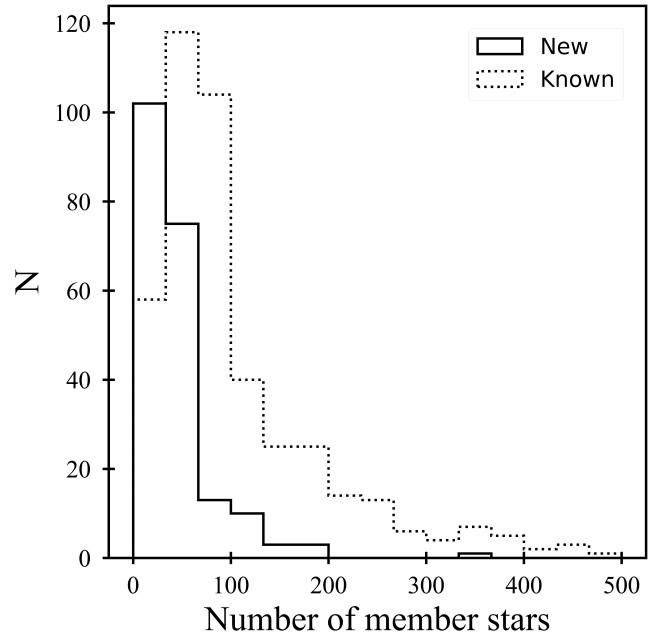


Figure 10. Frequency distribution of numbers of member stars. Solid lines represent newly discovered clusters, dotted lines represent known clusters.

the cluster. The relatively low central concentrations and small numbers of member stars of the new clusters caused their late detection.

The age distribution of the newly found clusters shows that the majority of them are intermediate-age open clusters. We found that some clusters have a significant number of member stars far from the center of the cluster. These clusters are thought to have extended halos or stars escaping from their gravitational potentials. There are a number of clusters that have elongated shapes. Some of them show multiple parallax peaks which suggest multiple components. However, the reason for the elongation is not clear. Dynamical evolution may play a critical role since most of these clusters are intermediate-age clusters. If the elongated shape originated from their formation process, we expect to find more elongated structures in younger clusters. Dynamical modeling is required to understand the origin of the elongated morphology.

ACKNOWLEDGMENTS

We are grateful to the anonymous referees for valuable comments and suggestions. This work has made use of data from the European Space Agency (ESA) mission *Gaia* (<https://www.cosmos.esa.int/gaia>), processed by the *Gaia* Data Processing and Analysis Consortium (DPAC, <https://www.cosmos.esa.int/web/gaia/dpac/consortium>). Funding for the DPAC has been provided by national institutions, in particular the institutions participating in the *Gaia* Multilateral Agreement. We also thank the Ulsan Science High School (USHS) for financial support. SGH would like to thank USHS science and mathematics teachers for help with understanding the theoretical background, especially

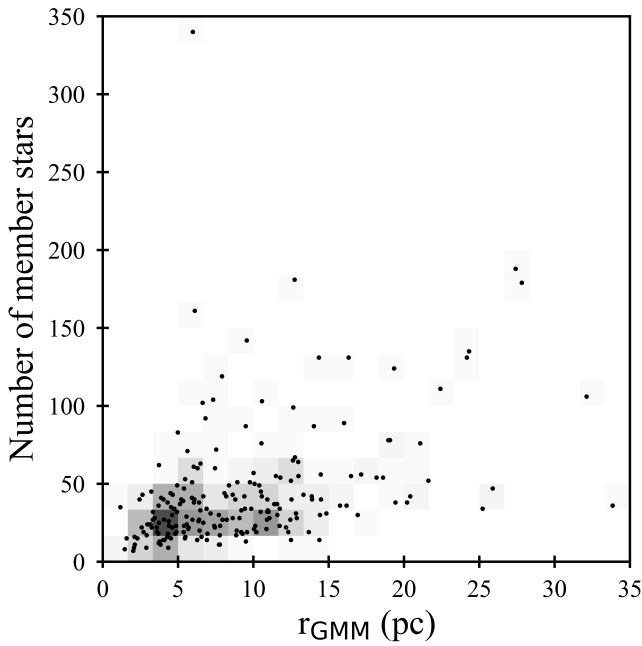


Figure 11. Number of member stars as a function of r_{GMM} .

Park Joo-Hyun. This work was partially supported by the 2018 Science and Technology Promotion Fund and Lottery Fund through KOFAC.

REFERENCES

- Ann, H. B., Lee, M. G., Chun, M. Y., et al. 1999, BOAO Photometric Survey of Galactic Open Clusters. I. Berkeley 14, Collinder 74, Biurakan 9, and NGC 2355, *JKAS*, 32, 7
- Bressan, A., Marigo, P., Girardi, L., et al. 2012, PARSEC: Stellar Tracks and Isochrones with the Padova and Trieste Stellar Evolution Code, *MNRAS*, 427, 127
- Camargo, D., Bica, E., & Bonatto, C. 2015, New Galactic Embedded Clusters and Candidates from a WISE Survey, *New Astron.*, 34, 84
- Camargo, D., Bica, E., Bonatto, C., et al. 2015, Discovery of Two Embedded Clusters with WISE in the High Galactic Latitude Cloud HRK 81.4-77.8, *MNRAS*, 448, 1930
- Cantat-Gaudin, T., Jordi, C., Vallenari, A., et al. 2018, A Gaia DR2 View of the Open Cluster Population in the Milky Way, *A&A*, 618, A93
- Cantat-Gaudin, T., Krone-Martins, A., Sedaghat, N., et al. 2019, Gaia DR2 Unravels Incompleteness of Nearby Cluster Population: New Open Clusters in the Direction of Perseus, *A&A*, 624, A126
- Castro-Ginard, A., Jordi, C., Luri, X., et al. 2018, A New Method for Unveiling Open Clusters in Gaia – New Nearby Open Clusters Confirmed by DR2, *A&A*, 618, A59
- Chen, W.-P., Chen, C., & Shu, C. 2004, Morphology of Galactic Open Clusters, *AJ*, 128, 2306
- Cheng, Y., 1995, Mean Shift, Mode Seeking, and Clustering, *IEEE Transactions on Pattern Analysis and Machine Intelligence*, 17, 790
- Chumak, Y. O., Platais, I., McLaughlin, D. E., et al. 2010, Numerical Simulations of Tidal Tails for the Open Cluster NGC 188, *MNRAS*, 402, 1841
- Dias, W., Alessi, B., Moitinho, A., et al. 2002, New Catalogue of Optically Visible Open Clusters and Candidates, *A&A*, 389, 871
- Evans, D., Riello, M., De Angeli, F., et al. 2018, Gaia Data Release 2 – Photometric Content and Validation, *A&A*, 616, A4
- Friel, F. D. 1995, The Old Open Clusters of the Milky Way, *ARA&A*, 33, 381
- Frinchaboy, P. M. & Majewski, S. R. 2008, Open Clusters as Galactic Disk Tracers. I. Project Motivation, Cluster Membership, and Bulk Three-dimensional Kinematics, *AJ*, 136, 118
- Froebrich, D., Scholz, A., & Raftery, C. 2006, A Systematic Survey for Infrared Star Clusters with $|b| < 20^\circ$ Using 2MASS, *MNRAS*, 374, 399
- Gaia Collaboration, Prusti, T., de Bruijne, J. H. J., et al. 2016, The Gaia Mission, *A&A*, 595, A1
- Gaia Collaboration, Brown, A. G., Vallenari, A. et al. 2016, Gaia Data Release 1 – Summary of the Astrometric, Photometric, and Survey Properties, *A&A*, 595, A2
- Gaia Collaboration, Brown, A. G. A., Vallenari, A., et al. 2018, Gaia Data Release 2 – Summary of the Contents and Survey Properties, *A&A*, 616, A1
- Gieles, M., Zwart, S. P., Baumgardt, H., et al. 2006, Star Cluster Disruption by Giant Molecular Clouds, *MNRAS*, 371, 793
- Janes, K. & Adler, D. 1982, Open Clusters and Galactic Structure, *ApJS*, 49, 425
- Janes, K. A. & Phelps, R. L. 1994, The Galactic System of Old Star Clusters: The Development of the Galactic Disk, *AJ*, 108, 1773
- Kharchenko, N. 2001, All-sky Compiled Catalogue of 2.5 Million Stars, *Kinematika i Fizika Nebesnykh Tel*, 17, 409
- Kharchenko, N., Piskunov, A., Rser, S., et al. 2005, 109 New Galactic Open Clusters, *A&A*, 440, 403
- Kharchenko, N., Berczik, P., Petrov, M., et al. 2009, Shape Parameters of Galactic Open Clusters, *A&A*, 495, 807
- Kharchenko, N., Piskunov, A., Schilbach, E., et al. 2013, Global Survey of Star Clusters in the Milky Way – II. The Catalogue of Basic Parameters, *A&A*, 558, A53
- King, I. R. 1966, The Structure of Star Clusters. IV. Photoelectric Surface Photometry in Nine Globular Clusters, *AJ*, 71, 276
- Koposov, S. E., Belokurov, V., & Torrealba, G. 2017, Gaia 1 and 2. A Pair of New Galactic Star Clusters, *MNRAS*, 470, 2702
- Krone-Martins, A., & Moitinho, A. 2014, UPMASK: Unsupervised Photometric Membership Assignment in Stellar Clusters, *A&A*, 561, A57
- Kroupa, P. 2001, On the Variation of the Initial Mass Function, *MNRAS*, 322, 231
- Kroupa, P. 2002, The Initial Mass Function of Stars: Evidence for Uniformity in Variable Systems, *Science*, 295, 82
- Lee, S., Kang, Y.-W., & Ann, H. B. 2013, Deep and Wide Photometry of Two Open Clusters NGC 1245 and NGC 2506: Dynamical Evolution and Halo, *MNRAS*, 432, 1672
- Lindgren, L., Hernández, J., Bombrun, A., et al. 2018, Gaia Data Release 2 – The Astrometric Solution, *A&A*, 616, A2
- Lynga, G., 1987, Catalog of Open Star Cluster Data, Strasbourg, CDS
- Mermilliod, J.-C. 1981, Comparative Studies of Young Open Clusters. III – Empirical Isochronous Curves and the Zero Age Main Sequence, *A&A*, 97, 235
- Mermilliod, J.-C., Egret, D., & Albrecht, M. 1995, Information and On-line data in Astronomy, 127 (Dordrecht: Kluwer Academic Press)

- Michie, R. W. 1964, *The Dynamics of Star Clusters*, *ARA&A*, 2, 49
- Oliveira, R. A. P., Bica, E., & Bonatto, C. 2018, Near-infrared Study of New Embedded Clusters in the Carina Complex, *MNRAS*, 476, 842
- Oort, J. H., 1979, Luminosity Distribution and Shape of the Hyades Cluster, *A&A*, 78, 312
- Pedregosa, F., Varoquaux, G., Gramfort, A., et al. 2011, Scikit-learn: Machine Learning in Python, *J. Machine Learning Research*, 12, 2825
- Piskunov, A. E., Just, A., Kharchenko, N. V., et al. 2018, Global Survey of Star Clusters in the Milky Way. VI. Age Distribution and Cluster Formation History, *A&A*, 614, 22
- Raboud, D. & Mermilliod, J.-C. 1998, Investigation of the Pleiades Cluster. IV. The Radial Structure, *A&A*, 329, 101
- Röser, S., Demleitner, M., & Schilbach, E. 2010, The PP-MXL Catalog of Positions and Proper Motions on the ICRS. Combining USNO-B1.0 and the Two Micron All Sky Survey (2MASS), *AJ*, 139, 2440
- Röser, S., Schilbach, E., & Goldman, B. 2016, Nine New Open Clusters within 500 pc from the Sun, *A&A*, 595, A22
- Röser, S., Schilbach, E., & Goldman, B. 2019, Hyades Tidal Tails Revealed by Gaia DR2, *A&A*, 621, L2
- Ryu, J. & Lee, M. G. 2018, A WISE Survey of New Star Clusters in the Central Plane Region of the Milky Way, *ApJ*, 856, 152
- Sandage, A. 1957, Observational Approach to Evolution. III. Semiempirical Evolution Tracks for M67 and M3, *ApJ*, 126, 326
- Scholz, R.-D., Kharchenko, N., Piskunov A., et al. 2015, Global Survey of Star Clusters in the Milky Way – IV. 63 New Open Clusters Detected by Proper Motions, *A&A*, 581, A39
- Skrutskie, M., Cutri, R., Stiening R., et al. 2006, The Two Micron All Sky Survey (2MASS), *AJ*, 131, 1163
- Terlevich, E. 1987, Evolution of N-body Open Clusters, *MNRAS*, 224, 193
- Trumpler, R. J. 1930, Preliminary Results on the Distances, Dimensions and Space Distribution of Open Star Clusters, *Lick Observatory Bulletin*, 14, 154
- Trumpler, R. J. 1931, *Star Clusters: A Review*, *PASP*, 43, 145